A&A 450, 15–23 (2006)
DOI: 10.1051/0004-6361:20054045
© ESO 2006

Astronomy & Astrophysics

Circumnuclear star-forming activities along the Hubble sequence⋆

L. Shi, Q. S. Gu⋆⋆, and Z. X. Peng

Department of Astronomy, Nanjing University, Nanjing 210093, PR China
e-mail: shileiastro@yahoo.com; qsgu@nju.edu.cn

Received 13 August 2005 / Accepted 5 December 2005

ABSTRACT

In order to study circumnuclear star-forming activity along the Hubble sequence, we cross-correlated the Sloan Digital Sky Survey Data Release 2 (SDSS DR2) with the Third Reference Catalog of Bright Galaxies (RC3) to derive a large sample of 1015 galaxies with both morphological and spectral information. Among these, 385 sources are classified as star-forming galaxies, and the SDSS fibre covered the circumnuclear regions (0.2−2.0 kpc). By using the spectral synthesis method to remove the contribution from the underlying old stellar population, we measured the emission lines fluxes accurately, which are then used to estimate the star-formation rates(SFRs). Our main findings are: (1) early-type spirals show much higher Hα luminosities, and hence higher SFRs, and also suffer more extinctions than late-type ones. The equivalent widths (*EW*s) of Hα emission lines show a similar trend; however, the very late types (Sdm ∼ Irr) do have large fractions of high *EW*s; (2) we confirm that $D_n(4000)$ shows a strong correlation with the strengths of metallic absorption lines (such as CN band, G band, and Mg Ib). Both these lines and the Balmer absorption lines show interesting variations between Sbc and Sd type galaxies; (3) the bar structure tightly relates to the enhanced star formation activity, an effect that is even more significant in the early-type spirals. But we should note that the bar structure is not a necessary or sufficient condition for galaxies to harbor circumnuclear star formations.

Key words. Galaxy: general – galaxies: stellar content – galaxies: statistics

1. Introduction

The history of star formation is one of the most important elements needed for understanding the evolution of the galaxies and also the universe. Enormous progress has been made during the last two decades. More precise diagnostics of global star-formation rates (SFRs) have been obtained in a broad range of techniques: e.g., integrated optical emission line fluxes (Kennicutt 1983; Kennicutt et al. 1994; Madau et al. 1998), near-ultraviolet continuum fluxes (Donas & Deharveng 1984; Deharveng et al. 1994; Madau et al. 1998; Bell & Kennicutt 2001), infrared continuum fluxes (Harper & Low 1973; Rieke & Lebofsky 1978; Telesco & Harper 1980; Kennicutt et al. 1987), and radio emissions (Condon 1992; Cram et al. 1998). Kennicutt (1998) offers an excellent review of star formation along the Hubble sequence.

A galaxy's morphology carries important information for the study of star formation in galaxies (e.g., Kennicutt 1998). The Hubble sequence (Hubble 1926), as one of the most widely used galaxy classifications, is closely connected with the overall star-forming activities of galaxies. The basic view of global SFRs along the Hubble sequence shows that the equivalent widths (*EW*s) of Hα emission lines increase from virtually zero in E/S0 galaxies to about a couple hundred Å in late-type spiral and irregular galaxies (Kennicutt & Kent 1983; Kennicutt 1998). However, recent studies of Hα imaging indicate that a significant fraction of the early-type spirals show remarkable star-formation activities (Young et al. 1996; James et al. 2004; Hameed & Devereux 2005).

Many galaxies have been shown to harbor luminous star-forming activities at the circumnuclear region with different properties from extended disks (Morgan 1958; Sérsic & Pastoriza 1967). Comprehensive surveys of the star-formation properties of galactic nuclei have been carried out both in the optical band (Stauffer 1982; Keel 1983; Kennicutt et al. 1989; Ho et al. 1997a,b) and with mid-IR photometry (Rieke & Lebofsky 1978; Scoville et al. 1983; Devereux et al. 1987; Giuricin et al. 1994). Ho et al. (1997a) found that the fraction of nuclear emission spectra with HII region-like line ratios increased from virtually zero in elliptical galaxies, 8% in S0 galaxies to 80% in Sc-Im galaxies. However, these could be contaminated by LINER or Seyfert nuclei.

In most galaxies, the nuclear SFRs are quite modest, while the highest SFRs are mainly seen in IR observations because the very luminous starbursts are mostly associated with dense molecular gas and have suffered substantial extinctions in the

⋆ Tables 4–7 are only available in electronic form at http://www.edpsciences.org

⋆⋆ Visiting Scholar, Harvard-Smithsonian Center for Astrophysics, 60 Garden St., Cambridge, MA 02138, USA.

Article published by EDP Sciences and available at http://www.edpsciences.org/aa or http://dx.doi.org/10.1051/0004-6361:20054045

optical band. The details of these IR luminous circumnuclear properties can be seen in Veilleux et al. (1995), Lutz et al. (1996), and also in Kennicutt (1998).

In this paper, we cross-correlate the largest spectral database available from the Sloan Digital Sky Survey (SDSS) and the Third Reference Catalog of Bright Galaxies (RC3) to derive a large sample of galaxies with both morphological and spectral information. We are thus able to statistically study the star-forming activities along the Hubble sequence. This paper is organized as follows: we describe the sample selection and also give a brief introduction to the stellar synthesis model in Sect. 2; the statistical results are presented in Sect. 3; in Sect. 4, we discuss bar influence on the star-formation activities; finally, we present our main conclusions in Sect. 5.

2. Sample

The Sloan Digital Sky Survey (SDSS, York et al. 2000; Stoughton et al. 2002; Abazajian et al. 2003) is one of the most ambitious surveys because it aims to obtain nearly 10^6 galaxies and 10^5 quasars when completed. This offers a great opportunity to explore the relations between the star-forming properties and their morphologies. We thus cross-correlate the SDSS galaxies (Data Release 2, Abazajian et al. 2004) with the RC3 catalog using the position-matching accuracy of 1 arcmin for most galaxies and 3 arcmin for those without enough accurate positions in RC3 (see the introduction of RC3).

We derived 983 galaxies with an average of positional differences of 0.0749 ± 0.052 arcmin, 11 galaxies with 0.7246 ± 0.1716 arcmin, and 33 galaxies with 2.055 ± 0.9156 arcmin. For those 44 galaxies with large positional differences, we checked one by one by using Sloan Digital Sky Survey/SkyServer[1]. Finally, we excluded 12 galaxies to avoid confusion and derived a sample of 1015 galaxies, 39 of which were defined as AGNs in Véron-Cetty & Véron (2003), so they too were excluded for further analysis. We derived consistent results by comparing our sample with NYU Value-Added Galaxy Catalog (Blanton et al. 2005)[2], where they present the SDSS galaxy catalog with RC3 information.

Since the SDSS spectrophotometry used the size-fixed fibre (3 arcsec), according to physical covering-size of the SDSS fibre, we divided the whole sample into three sub-samples that mainly depend on the SDSS fiber covering region size: (1) 33 sources in the nuclear sub-sample, where the fiber covers the region of less than 200 pc; (2) 824 sources in the circumnuclear sub-sample, where the fiber covers the region of 0.2 kpc $\sim$ 2 kpc; and (3) 119 sources in the disk sub-sample, where the fiber covers the region larger than 2 kpc. Just like most surveys, if not all, our sample will also suffer from the Malmquist bias. In the following we only concentrate on the circumnuclear sub-sample, with the relatively narrow redshift range of [0.00344, 0.0344], and also use the distance-independent parameters (such as *EW*s and Hα luminosity normalized by the fiber-covering size) as indicators of SFRs, both of which will reduce the Malmquist effect for this study.

[1] http://cas.sdss.org/astro/en/tools/search/

[2] http://wassup.physics.nyu.edu/vagc/

Table 1. The frequencies with different morphological types for the circumnuclear sample.

Galaxy type	E	L	S	Irr	Uncertain	Total
Number	43	127	536	18	100	824
Percentage	5.2	15.4	65.0	2.2	12.1	100

All galaxies were obtained from the cross-certification of RC3 and SDSS DR2 with the redshifts ranging from 0.0034 to 0.0344. The types were taken from the NED and calculated by using the definition of de Vaucouleurs et al. (1991).

Though RC3 (de Vaucouleurs et al. 1991) has been widely used in astrophysical research, much excellent work has been carried out in both photometric and spectroscopic observations ever since then, which has undoubtedly altered some galaxies' morphological classifications (such as in de Souza et al. 2004). As the NASA Extragalactic Database (NED) morphological types are the most up-to-date types in existence, we use them in this paper.

The results of cross-correlation between RC3 and SDSS DR2 for all 976 galaxies are shown in Table 4, which contains the galaxy name (Col. 1); RA and Dec (2000, Cols. 2−3); redshift (Col. 4); stellar and nebular extinctions (Cols. 5−6); luminosity of far-IR, in units of erg s^{-1} (Col. 7); morphology from NED (Col. 8).

Here we have combined all the elliptical galaxies into index $T = -2$, and included peculiar ones as Irregular galaxies ($T = 10$) by simply assuming that they may all be involved in various merger processes. The index $T = 13$ is set for the uncertain or unusual galaxies and are excluded from the statistical studies. Table 1 gives the number of each main branch of Hubble sequences for the circumnuclear sample, which contains 43 ellipticals, 127 lenticulars, 536 spirals, and 18 irregulars. Like most, if not all, galaxy samples, the current circumnuclear sample of galaxies can't be considered complete. We hope that the much larger number of galaxies can reduce the problem of incompleteness.

In most normal galaxies, stellar light dominates the continuum and absorption lines in the optical band. These absorption features can certainly contaminate the nebular emissions, which will be useful for understanding the physical properties of galaxies. Moreover, the stellar spectrum alone may provide direct measurements of the stellar population, velocity dispersion, star-formation history (SFH), etc. Thus how to properly decompose the stellar component from the integrated spectrum becomes the first step in interpreting the nuclear properties.

We use the stellar population synthesis code provided by Roberto Cid Fernandes, called *starlight V2.0*, for spectra synthesis, which fits an observed spectrum O_λ with a linear combination of $N_\star$ simple theoretical stellar populations (SSP) computed with the evolutionary synthesis models of Bruzual & Charlot (2003, BC03). The methodology of the code is described in detail by Cid Fernandes et al. (2004b). In this work we adopt a base with $N_\star = 45$ SSPs, with 3 metallicities: $Z = 0.2$, 1, and 2.5 $Z_\odot$, each of which has 15 ages ranged as 0.001, 0.003, 0.005, 0.01, 0.025, 0.04, 0.10, 0.29, 0.64, 0.90, 1.4, 2.5, 5.0, 11, and 13 Gyr. The match between model and

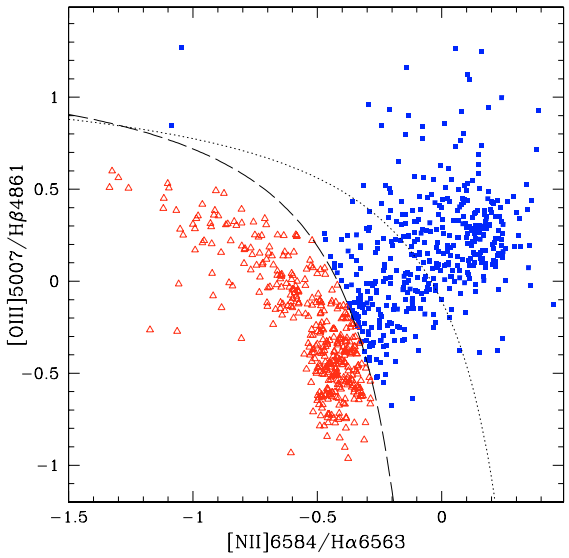

Fig. 1. The distribution of the galaxies in our circumnuclear sample in the BPT emission line ratio diagram. The dotted line is from Kewley et al. (2001), and the long-dashed line from Kauffmann et al. (2003), which will be used in this paper as the criteria to distinguish star-forming galaxies from the AGNs/composite sources. The filled rectangles show the AGNs/composite sources; while the open triangles represent the star-forming galaxies.

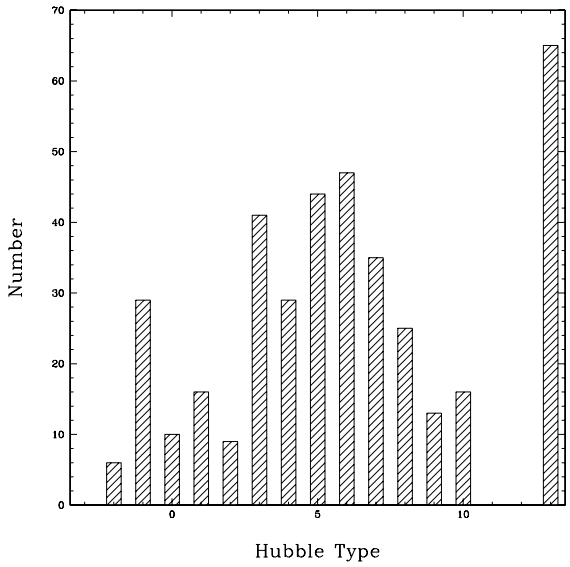

Fig. 2. The morphological distribution for the 385 star-forming galaxies. We set the T-index of those galaxies with uncertain types as $T = 13$.

observed spectrum is evaluated by $\chi^2 = \sum_\lambda [(O_\lambda - M_\lambda)\, w_\lambda]^2$, where w_λ^{-1} is the error in O_λ. The search for the best solution (also a minimum χ^2) is carried out by using a simulated annealing plus a Metropolis scheme (see Cid Fernandes et al. 2001, for a detail). Spectral regions around emission lines, bad pixels, and sky residuals are masked by setting $w_\lambda = 0$.

The spectra are first rebinned to 1 Å bins and redshift-corrected to the rest-frame by the standard IRAF[3] procedures. Then we correct the spectra for Galactic extinction using the reddening law of Cardelli et al. (1989) and the A_B values listed in NED (Schlegel et al. 1998) before starting the synthesis. We normalize the SSP basses at $\lambda_0 = 4020$ Å, while for the observed spectra we use the median value between 4010 and 4060 Å. Every spectrum has been synthesized from 3650 to 8000 Å.

Since in this paper we only concentrate on the star-forming galaxies, we use the criteria given by Kauffmann et al. (2003) to distinguish the potential AGNs and the composite (AGN+starburst) sources from star-forming galaxies. Figure 1 is the diagram from Baldwin et al. (1981, BPT) applied to our sample. After adopting the line of Kauffmann et al. (2003), we derive 385 star-forming galaxies and 438 AGNs/composite sources. There is still one galaxy not presented in this diagram, because it shows no emission-line features in either its original spectrum or the continuum subtracted one. Figure 2 shows the morphological distribution for these star-forming galaxies.

[3] IRAF is distributed by the National Optical Astronomy Observatory, which is operated by the Association of Universities for Research in Astronomy, Inc., under cooperative agreement with the National Science Foundation.

Table 2. Definitions of emission-line windows.

Emission lines	Windows	Continuum windows
Hδ 4101	4090–4114	4055–4065 4135–4145
Hγ 4340	4328–4352	4250–4260 4400–4410
HeII 4686	4672–4700	4655–4665 4720–4730
Hβ 4861	4851–4871	4825–4835 4885–4895
[OIII] 4959	4949–4969	4915–4925 5035–5045
[OIII] 5007	4997–5017	4915–4925 5035–5045
Hα 6563	6556–6573	6520–6530 6610–6620

All wavelengths are in units of Å.

3. Statistic results

3.1. Emission line features

We have measured the emission line features from the "pure emission" spectra, which are derived by subtracting synthetic spectrum from the observed one. The measurement is automatic, and the windows for emission line and continuum are listed in Table 2.

The Hα luminosities of the sample span a large range from about 10^{37} to 10^{42} erg s^{-1} (Fig. 3). The early-type (S0−Sbc) spirals extend much farther toward the high end of L(Hα) than do the late-type (Sc−Im) ones[4], which is consistent with Ho et al. (1997a). The median value of $\log(L[\mathrm{H}\alpha])$ is 40.02 and 39.14 for the early-type and late-type galaxies, respectively. We should note that this trend truly exists and is slightly exaggerated by the effect of nebular extinctions. Table 5 shows the flux densities of Hβ 4861 (Col. 2), [OIII] 5007 (Col. 3), [NII] 6548, 6584 (Cols. 4−5), Hα 6563 (Col. 6), and [SII] 6717, 6731 (Cols. 7−8) for our sample, all in units of 10^{-17} erg s^{-1} cm^{-2}.

[4] From here to the end of this paper, the early-type refers to S0/a−Sbc and the late-type refers to Sc−Sm as in Ho et al. (1997a,b).

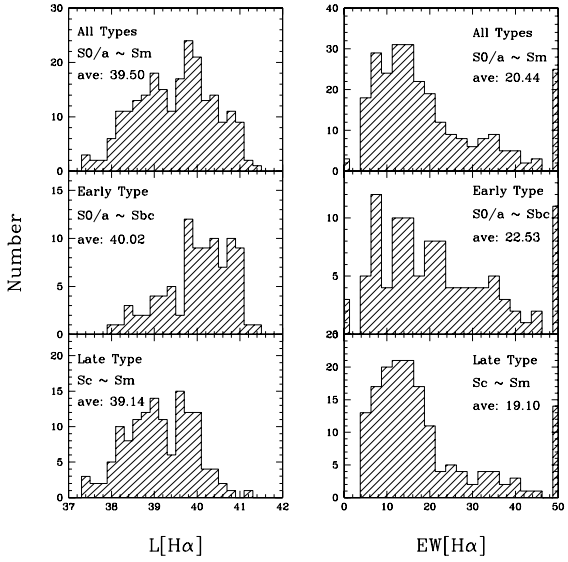

Fig. 3. The histogram of extinction-corrected $L(\mathrm{H}\alpha)$ and $EW(\mathrm{H}\alpha)$. *From the top to bottom* are the distributions of Hα luminosities and equivalent widths for all galaxies, early-type, and late-type ones, respectively. The luminosities have all been corrected for Balmer extinction.

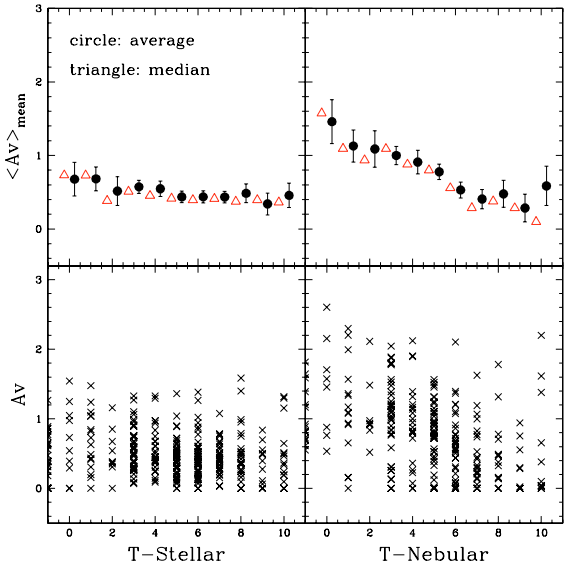

Fig. 4. The distribution of extinction along the Hubble sequence. *The two left panels* are the distributions of stellar extinctions (*bottom panel*) and their median (open triangles) and average values (filled circles). The error bar represents the deviation in the mean. The right plots are for the nebular extinctions.

Corresponding equivalent widths are shown in Table 6 for all the sample galaxies, in units of Å.

3.2. Extinction

The dust extinction can have a considerable impact on the thermal balance of the interstellar medium and on the formation of H_2 molecules, which have important consequences on the efficiency of star formation (Omukai 2000; Hirashita & Ferrar 2002). The nebular extinction is derived from the observed Balmer decrement (Hα/Hβ, see Torres-Peimbert et al. 1989). Assuming Case B recombination and a standard reddening law (Cardelli et al. 1989), we obtain the V-band extinction:

$$A_{\mathrm{V}}^{\mathrm{nebular}} = 6.31 \times \log\left(\frac{F_{\mathrm{H}\alpha}/F_{\mathrm{H}\beta}}{I_{\mathrm{H}\alpha}/I_{\mathrm{H}\beta}}\right), \quad (1)$$

where $F_{\mathrm{H}\alpha}/F_{\mathrm{H}\beta}$ and $I_{\mathrm{H}\alpha}/I_{\mathrm{H}\beta}$ are the observed and intrinsic flux ratios of Hα and Hβ, respectively. Here we use the intrinsic ratio of $I_{\mathrm{H}\alpha}/I_{\mathrm{H}\beta}$ to be 2.86 (Osterbrock 1989). Galaxies where either of the two lines is insufficient in fluxes (less than 3σ) were excluded here. We also derived some negative values of A_{V}. Since these were unexpected for the common model of extinction and may actually be overestimated (see Cid Fernandes et al. 2005, for the details), we set them as zero when studying the relation between the extinctions and Hubble types, and also in the previous study of Hα luminosities.

It is believed that emission lines suffer more extinctions than stellar light (Calzetti et al. 1994; Gordon et al. 1997; Mas-Hesse & Kunth 1999). More recently, Cid Fernandes et al. (2005) apply the synthesis model to a large number of SDSS galaxies and get a linear bisector fitting $A_V^{\mathrm{Balmer}} = 0.24 + 1.81A_V$. Since we use the same code as Cid Fernandes et al. (2005), it is not surprising that we derive similar results.

Figure 4 shows the distribution of both the stellar and nebular extinctions (A_V) along the Hubble sequence. We find that the nebular extinction decreases from early-type spirals to late-type spirals, which is consistent with Ho et al. (1997a) and Stasińska et al. (2004), while the trend of the stellar extinction is almost flat with slight variations among morphology types. This is accessible, since the stellar extinction represents the comparably old stars that are believed to have exposed from the surrounding molecular clouds.

3.3. Star-formation rates

We calculate the star-formation rate from the extinction-corrected Hα luminosity using Kennicutt's (1998) conversion,

$$SFR\ (M_\odot\ \mathrm{yr}^{-1}) = 7.9 \times 10^{-42}\ L(\mathrm{H}\alpha)\ (\mathrm{ergs\ s}^{-1}), \quad (2)$$

Here we get an average SFR of 0.14 $M_\odot\,\mathrm{yr}^{-1}$ with a median value of 0.04 $M_\odot\,\mathrm{yr}^{-1}$ for those galaxies with A_{V} or with no sufficient fluxes in both Hα and Hβ lines that would be set as zero in the SFRs of our 385 galaxies. These values are consistent with Ho et al. (1997a). Figure 5 (top) shows the distribution of star-formation rates as a function of Hubble T-types. We find that the spiral galaxies of type Sb show the highest star-formation rate, which is slightly different from the global properties of the Hα survey (James et al. 2004, peaking at Sbc and Sc). A clear trend exists along the Hubble types with the values of SFR(Hα) decreasing from early-type spirals to the late-type ones (Fig. 5, bottom). This is consistent with Stauffer (1982), Keel (1983), and Ho et al. (1997a). Many works emphasize the aperture effect, while here we just normalize the SFR by the corresponding aperture areas. This simple process will undoubtedly induce some bias; however, it is worth to see the general trend. Figure 6 shows the trend of SFRs per kpc^2

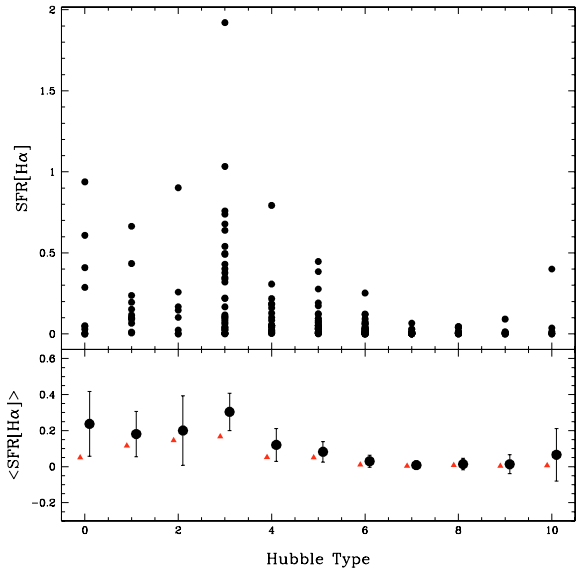

Fig. 5. The circumnuclear SFRs of Hα along the Hubble sequence. Most galaxies show moderate SFRs, while large dispersions are seen in early-type galaxies. The median SFR values show a clear trend decreasing from early-type to late-type spirals. Symbols have the same meaning as in Fig. 4.

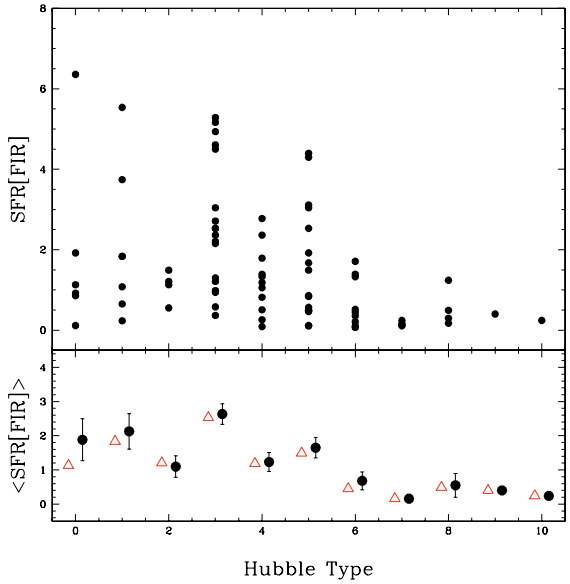

Fig. 7. The distribution of FIR SFRs among Hubble types. The early-type spirals show comparably higher values; however, this may be due to the lack of data in late-type spirals. Symbols have the same meaning as in Fig. 4.

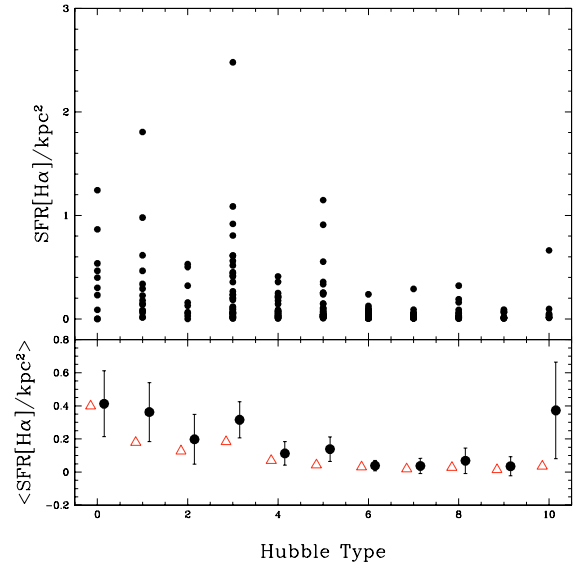

Fig. 6. The distribution of SFRs normalized by the aperture areas. The trend is much weaker, although the early-type galaxies do show higher median values of SFR(Hα).

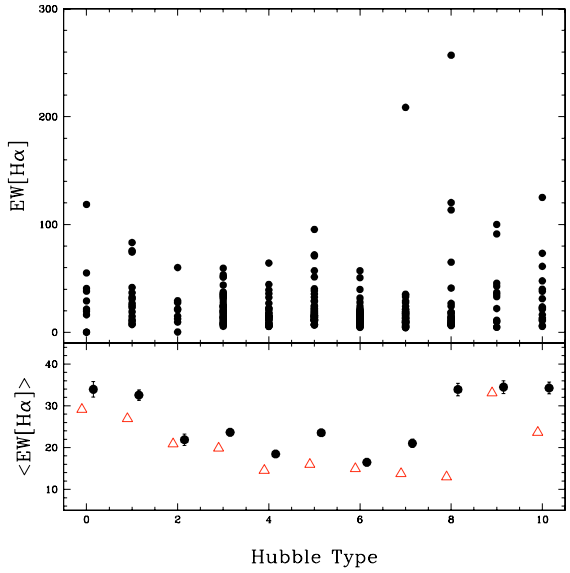

Fig. 8. The distribution of EW(Hα) among the Hubble types. There is no significant trend found with morphology types, although the late-type galaxies do show comparably larger dispersions and higher median values. The triangles represent the median values and the filled circles are the averages, which may be affected by the few extremely higher ones.

along the Hubble sequence. Though it is slightly weaker, we still find that early-type spirals do show higher SFRs kpc^{-2} than the late-type spirals. Thus while luminous nuclear starbursts may exist in the entire range of spirals (Rieke & Lebofsky 1978; Devereux 1987), the relative effect is much stronger for early-type spirals. We also calculated the SFRs from the far-infrared emissions available in the RC3. Figure 7 shows the FIR-SFRs along the Hubble types. Again, we find that the early-type spirals do show higher SFRs but do not significantly exceed those of late types.

The equivalent width of Hα (EW[Hα]), which represents the efficiency of the star-forming activity, shows a similar result (Fig. 3). In Fig. 8, we present the variations of EWs among the Hubble types. We find that early-type spirals show large equivalent widths (EWs), especially for the S0/a ~ Sab galaxies. From Sbc to Sd type, galaxies show similar EWs, and for the end of the sequence (Sdm ~ I) we clearly see a large fraction of high equivalent widths.

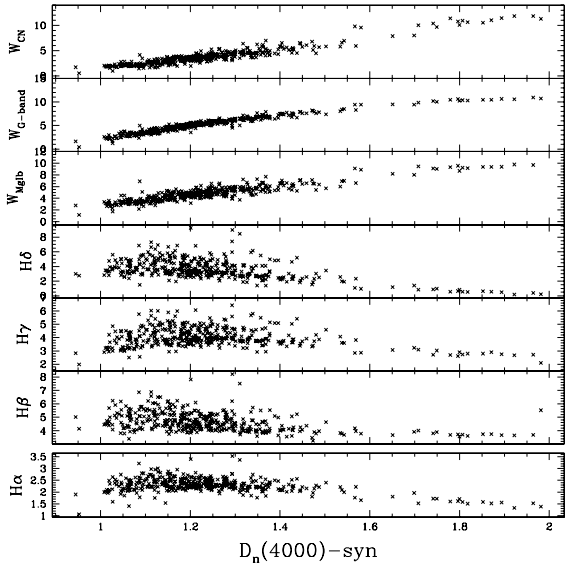

Fig. 9. Relations between $D_n(4000)$ and equivalent widths of CN band, G band, Mg Ib, Hδ, Hγ, Hβ, and Hα measured in the synthetic spectrum. Correlations are clearly seen in almost all diagrams; however, the first three metal absorptions (*top*) show the strongest.

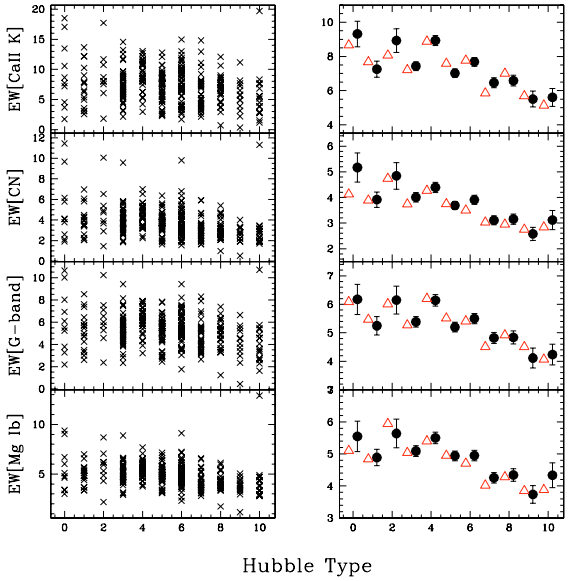

Fig. 10. Relations between Hubble types and equivalent widths of CaII K, CN band, G band, and Mg Ib lines measured in the synthetic spectrum. A decreasing trend exists from early-type spirals to the late-type, especially for those later than Sbc. Symbols have the same meaning as in Fig. 4.

For all Hubble types, the moderate values of both SFRs and *EW*s of Hα are very common in the distributions, although large dispersion do exit within the same type, which is consistent with James et al. (2004). Furthermore, we also find that some elliptical and lenticular galaxies show considerably high *SFR*(Hα) and *EW*(Hα). Since Hα emission has a different origin in ellipticals and S0's than in spiral galaxies, which is usually due to the nuclear activities or merger/peculiar interactions, we will not discuss these ellipticals and S0's in this paper.

3.4. Stellar features

We measured a set of stellar indices directly from the synthetic spectra. For most of the stellar features, we used the same indices as defined by Cid Fernandes et al. (2004a), which are based on the studies of star cluster and galaxy spectra by Bica & Alloin (1986a,b) and Bica (1988). We adopted the definition of Worthey & Ottaviani (1997) and Balogh et al. (1999) for Hδ_A and $D_n(4000)$, respectively. The results of the absorption lines are presented in Table 7: *EW*s of CaII K 3933 (Col. 2), CN band 4200 (Col. 3), G band 4300 (Col. 4), Mg Ib 5173 (Col. 5), Hδ 4101 (Col. 6), Hγ 4340 (Col. 7), Hβ 4861 (Col. 8), Hα 6563 (Col. 9), and $D_n(4000)$ (Col. 10), all in units of Å.

During their study of SDSS galaxies, Kauffmann et al. (2003) find that $D_n(4000)$ is a useful indicator of stellar population, which has also been confirmed by the study of Seyfert 2 galaxies (Cid Fernandes et al. 2004b). In Fig. 9, we present the relations between $D_n(4000)$ and model-derived equivalent widths of 3 absorption lines in the Bica's system: CN band, G band, Mg Ib, and 3 Balmer absorption lines (Hβ, Hγ, and Hδ). The equivalent widths of CN band, G-band, and Mg Ib strongly correlate with $D_n(4000)$. The three Balmer lines also show some correlation that is not very tight.

One useful application of stellar population synthesis methods is to decompose the stellar contributions from the integrated spectrum to obtain pure nebular emission lines. Thus to derive accurate corrections of Balmer absorption features is particularly necessary. A previous study by McCall et al. (1985) recommended a mean absorption correction of 2 Å to the *EW*s for the first three Balmer lines. Veilleux et al. (1995) also obtained a correction 2 Å for *EW*(Hβ) of the old stellar population, ranging from 1 to 3 Å. More recently in the study of star-formation histories for a sample of starburst galaxies, Mayya et al. (2004) got the mean absorption *EW*s of 1.57, 2.48, 2.32, 2.49 Å for the first four Balmer lines. In our studies, the mean average Balmer absorption *EW*s of Hα, Hβ, Hγ and Hδ are 2.30, 4.68, 4.07, and 3.62, respectively.

Figures 10 and 11 show the distributions of 8 stellar absorption *EW*s: CaII K, CN band, G-band, Mg Ib, Hα, Hβ, Hγ, and Hδ along the Hubble types. The four metallic absorption features show a clear trend decreasing from the early-type spirals to late-type and irregular ones, especially for those later than Sbc. On the other hand, the four Balmer absorption lines exhibit an interesting increase from Sbc to Sd type galaxies, though all these variations are actually small. Thus, the correction due to the Balmer absorption features should not be considered as a completely uniform value, but rather as a variation among the Hubble types.

4. Bar's influence on the star-forming activity

Bar structures are well known for efficiently enhancing the star-formation activities of the circumnuclear regions (Huang et al. 1996; Ho et al. 1997b; Kennicutt 1998). Many numerical simulations predict that a bar can effectively drive the radial inflow of gas toward the center of a galaxy, which induces the burst

Table 3. The bar existence among different morphological types.

Galaxy type	L	S0/a	Sa	Sab	Sb	Sbc	Sc	Scd	Sd	Sdm	Sm	Irr
Normal	22	3	11	4	16	15	19	23	18	13	2	11
SAB	3	0	1	1	6	7	13	8	4	5	1	2
SB	4	7	4	4	19	7	12	16	13	7	10	3

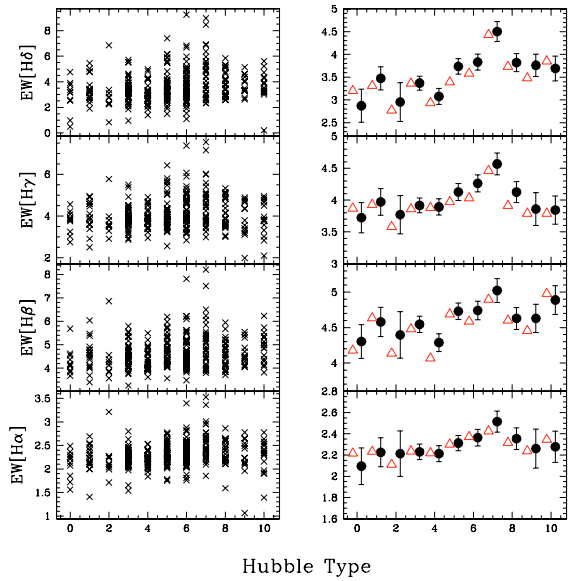

Fig. 11. Relations between Hubble types and equivalent widths Hδ, Hγ, Hβ, and Hα absorption lines measured in the synthetic spectrum. It is interesting to find that *EW*s increase from Sbc to Sd type in all Balmer absorption lines.

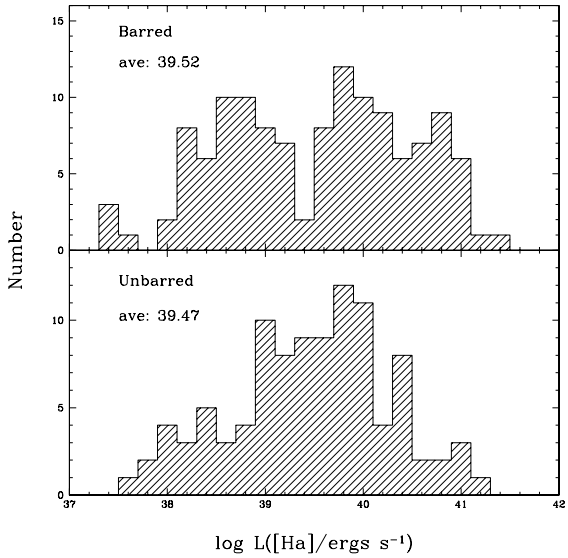

Fig. 12. Distribution of extinction − corrected Hα luminosities. *From top to bottom* are barred and unbarred galaxies. This interesting gap between the lower and higher Hα luminosity in barred galaxies also exists in Fig. 3 of Ho et al. (1997b).

of star formation (e.g., Roberts et al. 1979; Elmegreen 1988; Athanassoula 1992; Piner et al. 1995).

In all the 385 star-forming galaxies, 157 are non-barred galaxies, 51 are weak barred galaxies (SAB), and 106 contain strong bars (SB), ranging from lenticular to irregular galaxies. Thus we get an almost equal number of barred and unbarred galaxies in our sample; there are another 3 barred galaxies in the remaining 65 galaxies with uncertain morphologies, while the other 6 are elliptical galaxies. It is obvious that barred galaxies are very common in each Hubble type.

The comparison between Hα luminosities in barred and unbarred galaxies is shown in Fig. 12. The barred galaxies show a large fraction toward the high end of L(Hα). An interesting gap between high and low parts of luminosities also exists in Fig. 3 of Ho et al. (1997b). Figure 13 shows the distribution of both the individual galaxies and the mean star-formation rates of our sample, but this time separated into barred (filled circle) and unbarred (open triangle) types. It is clear that bars can enhance star formation, or at least extend the range toward the higher SFRs. This trend mainly occurs in the early-type spirals, which is consistent with previous studies of Huang et al. (1996) and Ho et al. (1997b). It is worth noting that the enhancement of central star formation in barred galaxies is a clear signature of secular disk evolution in action, which has been recently reviewed by Kormendy & Kennicutt (2004).

Less agreement is found in the distribution of *EW*(Hα)s (Fig. 14). In general, the equivalent widths of Hα in barred galaxies are higher than in unbarred ones, but not significant in many individual types. We do find clear enhancement in *EW*(Hα) of barred galaxies (Fig. 15); however, the largest difference is seen in the very late types. Since late-type spirals are believed to be gas-rich, then other influences such as gas content and interactions may also play an important role in the circumnuclear star-formation activities.

5. Conclusions

We constructed a sample of galaxies by position matching up the SDSS and RC3 data. We then applied the stellar population synthesis model to statistically study the variations of star-formation histories and line features among the Hubble types. Our findings are summarized as follows:

1. A decreasing sequence was found for nebular extinction from early-type spirals to late-type ones, which is consistent with previous studies by Ho et al. (1997a) and Stasińska et al. (2004). We also confirmed that nebular emissions do suffer more serious extinctions than stellar light, and the later one shows almost no variations among the Hubble types.
2. We find that Hα luminosities of early-type spiral galaxies are much higher than the late-type ones, which causes

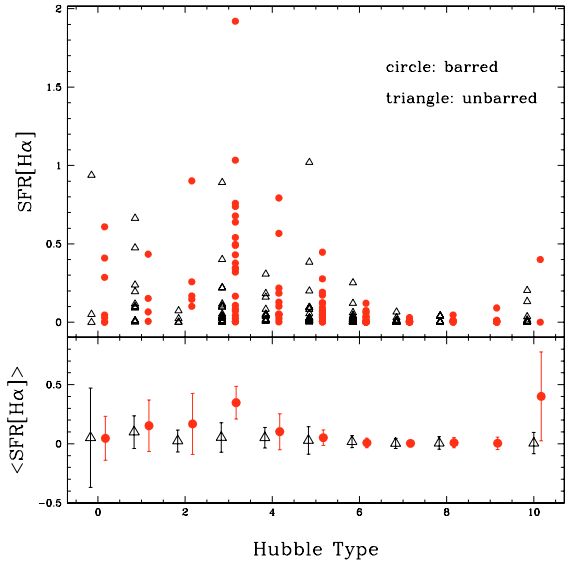

Fig. 13. The SFRs of barred and unbarred galaxies as a function of Hubble T-type. From top to bottom are the distribution of individual galaxies and their average values. Filled circles represent the barred galaxies, while the open triangles show the unbarred ones. The errorbar is the deviation in the mean value.

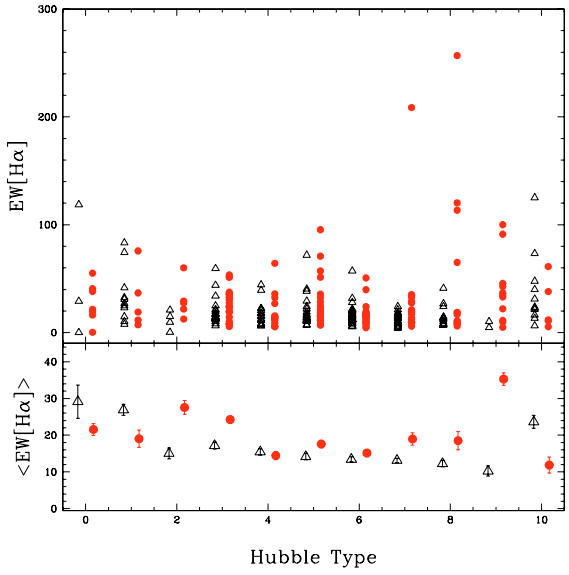

Fig. 14. The *EW*[Hα] of barred and unbarred galaxies as a function of Hubble T-type. *From top to bottom* are the distribution of individual galaxies and their average values. Symbols have the same meaning as in Fig. 13

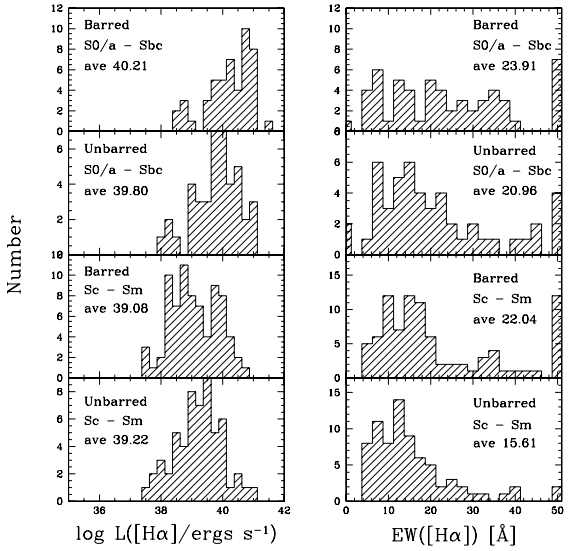

Fig. 15. The histograms of the extinction-corrected *L*[Hα] (*left*) and *EW*(Hα) (*right*). The two top panels show the barred and unbarred galaxies in early-type spirals (S0/a-Sbc) and the two bottoms show the late-type spirals (Sc-Sm).

the corresponding larger SFRs in early-type spirals. From the equivalent widths of Hα, we find in general that early-type spirals show a higher value for *EW*s; however, the dramatic change is found from Sdm type. We also plotted the FIR-SFRs as a function of Hubble types and found that the early-type spirals show higher amount of FIR-SFRs and may partly be due to the dust re-emission that will favor the early types. However, this difference of SFRs in the IR band is comparably much smaller. Although a large number of galaxies show quite modest SFRs and may not actually contain bright HII regions, those that do strongly favor the higher star-forming activities in early-type galaxies.

3. We measured the spectral absorption features and confirmed previous findings that tight correlations exist between $D_n(4000)$ and the equivalent widths of absorption lines: CN band, G-band, Mg Ib, Hδ, Hγ, Hβ, and Hα. The dependence of mean *EW*s on the Hubble types could be seen in metallic absorption lines. We also found an increase sequence of mean Balmer absorption equivalent widths from Sbc to Sd type. Since all these *EW*s are measured automatically, they do not depend on the morphology type.
4. We discussed the bar effects on the star-forming activities on both early-type and late-type spirals, and confirmed previous findings that bar structures can enhance star-forming activities, especially in early type spiral galaxies. However, bars do not necessarily induce strong star-formation activities; and those without could still contain regions of high star formation. We also find that, although in general the barred early-type spirals show larger *EW*[Hα], the largest difference of *EW*[Hα] between barred and unbarred galaxies exists in the very late-type spirals (Sd ~ Sm). Thus we believe that other effects like interactions and gas contents may also play important roles in star-formation activities.

Acknowledgements. We would like to thank the anonymous referee for instructive comments which improved the content of the paper and thank Roberto Cid Fernandes for sending us the updated code for stellar population synthesis. This work is supported by the National Natural Science Foundation of China under grant 10221001 and the National Key Basic Research Science Foundation (NKBRSG19990754). Funding for the creation and distribution of the SDSS Archive has been provided by the Alfred P. Sloan Foundation, the Participating Institutions, the National Aeronautics and Space Administration, the National Science Foundation, the US Department of Energy, the Japanese Monbukagakusho, and the Max

Planck Society. The SDSS web site is http://www.sdss.org/. The SDSS is managed by the Astrophysical Research Consortium (ARC) for the Participating Institutions. The Participating Institutions are The University of Chicago, Fermilab, the Institute for Advanced Study, the Japan Participation Group, The Johns Hopkins University, Los Alamos National Laboratory, the Max-Planck-Institute for Astronomy (MPIA), the Max-Planck-Institute for Astrophysics (MPA), New Mexico State University, University of Pittsburgh, Princeton University, the United States Naval Observatory, and the University of Washington. This research has made use of the NASA/IPAC Extragalactic Database (NED) which is operated by the Jet Propulsion Laboratory, California Institute of Technology, under contract with the National Aeronautics and Space Administration.

References

Abazajian, K., Adelman-McCarthy, J. K., Agüeros, M. A., et al. 2003, AJ, 126, 2081A
Abazajian, K., Adelman-McCarthy, J. K., Agüeros, M. A., et al. 2004, AJ, 128, 502A
Athanassoula, E. 1992, MNRAS, 259, 345
Baldwin, J. A., Phillips, M. M., & Terlevich, R. 1981, PASP, 93, 5
Balogh, M., Morris, S., Yee, H., et al. 1999, ApJ, 527, 54
Bell, E. F., & Kennicutt, R. C. 2001, ApJ, 548, 681
Bica, E. 1988, A&A, 195, 76
Bica, E., & Alloin, D. 1986a, A&A, 162, 21
Bica, E., & Alloin, D. 1986b, A&A, 166, 83
Blanton, M. R., Schlegel, D. J., Strauss, M. A., et al. 2005, AJ, 129, 2562
Bruzual, G., & Charlot, S. 2003, MNRAS, 344, 1000
Calzetti, D., Kinney, A. L., & Storchi-Bergmann, T. 1994, ApJ, 429, 582
Cardelli, J. A., Clayton, G. C., & Mathis, J. S. 1989, ApJ, 345, 245
Cid Fernandes, R., Sodre, L., Schmitt, H. R., et al. 2001, MNRAS, 325, 60
Cid Fernandes, R., Delgado, R. M. G., Schmitt, H. R., et al. 2004a, ApJ, 605, 105
Cid Fernandes, R., Gu, Q., Melnick, J., et al. 2004b, MNRAS, 355, 273
Cid Fernandes, R., Mateus, A., Sodre, L., Stasinska, G., & Gomes, J. M. 2005, MNRAS, 358, 363
Condon, J. J. 1992, ARA&A, 30, 575
Cram, L., Hopkins, A., Mobasher, B., & Rowan-Robinson, M. 1998, ApJ, 507, 155
de Souza, R. E., Gadotti, D. A., & dos Anjos, S. 2004, ApJS, 153, 411
Deharveng, J. M., Sasseen, T. P., Buat, V., et al. 1994, A&A, 289, 715
de Vaucouleurs, G., de Vaucouleurs, A., Corwin, H. G., et al. 1991, Third Reference Catalogue of Bright Galaxies (New York: Springer) (RC3)
Devereux, N. A. 1987, ApJ, 323, 91
Devereux, N. A., Becklin, E. E., & Scoville, N. 1987, ApJ, 312, 529
Donas, J., & Deharveng, J. M. 1984, A&A, 140, 325
Elmegreen, B. G. 1988, ApJ, 326, 616
Giuricin, G., Tamburini, L., Mardirossian, F., Mezzetti, M., & Monaco, P. 1994, A&A, 427, 202
Gordon, K. D., Calzetti, D., & Witt, A. N. 1997, ApJ, 487, 625
Hameed, S., & Devereux, N. 2005, AJ, 129, 2597
Harper, D. A., & Low, F. J. 1973, ApJ, 182, L89
Hirashita, H., & Ferrara, A. 2002, MNRAS, 337, 921
Ho, L. C., Filippenko, A. V., & Sargent, W. L. W. 1997a, ApJ, 487, 579
Ho, L. C., Filippenko, A. V., & Sargent, W. L. W. 1997b, ApJ, 487, 591
Huang, J. H., Gu, Q. S., Su, H. J., et al. 1996, A&A, 313, 13
Hubble, E. 1926, ApJ, 64, 321
James, P. A., Shane, N. S., Beckman, J. E., et al. 2004, A&A, 414, 23
Kauffmann, G., Heckman, T., White, S., et al. 2003, MNRAS, 341, 33
Keel, W. C. 1983, ApJ, 269, 466
Kennicutt, R. C. 1983, ApJ, 272, 54
Kennicutt, R. C. 1998, ARA&A, 36, 189
Kennicutt, R. C., & Kent, S. M. 1983, AJ, 88, 1094
Kennicutt, R. C., Keel, W. C., van der Hulst, J. M., Hummel, E., & Roettiger, K. A. 1987, AJ, 93, 1011
Kennicutt, R. C., Keel, W. C., & Blaha, C. A. 1989, AJ, 97, 1022
Kennicutt, R. C., Tamblyn, P., & Congdon, C. W. 1994, ApJ, 435, 22
Kewley, L. J., Dopita, M. A., Sutherland, R. S., Heisler, C. A., & Trevena, J. 2001, ApJ, 556, 121
Kormendy, J., & Kennicutt, R. C. 2004, ARA&A, 42, 603
Lutz, D., Genzel, R., Sternberg, A., et al. 1996, A&A, 315, L137
Madau, P., Pozzetti, L., & Dickinson, M. 1998, ApJ, 498, 106M
Mas-Hesse, J. M., & Kunth, D. 1999, A&AS, 349, 765
Mayya, Y., Bressan, A., Rodríguez, M., Valdes, J. R., & Chavez, M. 2004, ApJ, 600, 188
McCall, M., Rybski, P., & Shields, G. 1985, ApJS, 57, 1
Morgan, W. W. 1958, PASP, 70, 364
Omukai, K. 2000, ApJ, 534, 809
Osterbrock, D. E. 1989, Astrophysics of Gaseous Nebulae and Active Galactic Nuclei (Mill Valley: University Science Books)
Piner, B. G., Stone, J. M., & Teuben, P. J. 1995, ApJ, 449, 508
Rieke, G. H., & Lebofsky, M. J. 1978, ApJ, 220, L37
Roberts, W. W., Huntley, J. M., & van Albada, G. D. 1979, ApJ, 233, 67
Schlegel, D. J., Finkbeiner, D. P., & Davis, M. 1998, ApJ, 520, 525
Scoville, N. Z., Becklin, E. E., Young, J. S., & Capps, R. W. 1983, ApJ, 271, 512
Sérsic, J. L., & Pastoriza, M. 1967, PASP, 79, 152
Stasińska, G., Mateus, A. Jr., Sodré, L. Jr., & Szczerba, R. 2004, A&A, 420, 475
Stauffer, J. R. 1982, ApJS, 50, 517
Stoughton, C., Lupton, R. H., Bernardi, M., et al. 2002, AJ, 123, 485
Telesco, C. M., & Harper, D. A. 1980, ApJ, 235, 392
Torres-Peimbert, S., Peimbert, M., & Fierro, J. 1989, ApJ, 345, 186
Veilleux, S., Kim, D.-C., Sanders, D. B., Mazzarella, J. M., & Soifer, B. T. 1995, ApJS, 98, 171
Véron-Cetty, M. P., & Véron, P. 2003, A&A, 412, 399V
Worthey, G., & Ottaviani, D. L. 1997, ApJS, 111, 377
York, D. G., Adelman, J., Anderson, J. E., Jr., et al. 2000, AJ, 120, 1579
Young, J. S., Allen, L., Kenney, J. D. P., Lesser, A., & Rownd, B. 1996, AJ, 112, 1903

Online Material

Table 4. Catalog of the whole sample.

Name	RA(2000)	Dec(2000)	Redshift	Av_{st}	Av_{neb}	log L^a_{FIR}	Morphology
NGC 3042	09h53m20.2s	+00d41m51.8s	0.012613	0.1073	- - -	- -	S0
UGC 5238	09h46m53.5s	+00d30m26.4s	0.005929	0.7515	0.7775	- -	SBdm
UGC 7963	12h47m52.9s	–01d11m08.9s	0.023371	0.9519	- - -	- -	Sdm
A1252+00	12h55m12.6s	+00d06m59.9s	0.004180	0.0295	0.5290	- -	SBd
NGC 4668	12h45m31.9s	–00d32m08.5s	0.005431	0.1912	0.3029	42.38	SBd
CGCG 15-20	12h47m19.3s	+00d24m17.4s	0.047169	–0.0587	- - -	- -	S0
MCG 0-29-27	11h24m08.6s	–01d09m27.9s	0.029288	0.5686	1.0296	- -	SAB0
UGC 6435	11h25m35.0s	–00d46m05.6s	0.025325	–0.0924	- - -	- -	S0
UGC 6340	11h19m55.4s	–00d52m47.9s	0.024573	–0.0535	- - -	43.65	SABbc
UGC 6432	11h25m17.9s	+00d21m01.8s	0.040292	0.2952	0.2812	- -	SAbc
CGCG 11-100	11h27m36.7s	+00d23m42.8s	0.049075	0.3285	- - -	- -	SBb
MCG 0-29-29	11h24m18.6s	+00d38m37.4s	0.026402	0.2049	1.3175	- -	SBc
UGC 9299	14h29m34.6s	–00d01m05.7s	0.005204	0.2909	–0.1752	- -	SABd
IC 1010	14h27m20.3s	+01d01m33.2s	0.025687	0.2471	- - -	- -	SBb
MCG 0-29-36	11h28m16.4s	+00d53m28.9s	0.039884	0.2740	0.7626	- -	SABbc
UGC 6402	11h23m19.1s	–00d55m21.4s	0.008698	0.9888	1.3155	43.04	Sdm
UGC 6457	11h27m12.2s	–00d59m40.8s	0.003191	0.5764	–0.0508	- -	dIn
MCG 0-30-4	11h31m58.6s	–00d03m01.1s	0.039859	0.7349	- - -	- -	SAcd
MCG 0-29-28	11h24m09.1s	+00d42m01.9s	0.025987	0.4158	0.0219	- -	Sc
NGC 3719	11h32m13.4s	+00d49m09.3s	0.019457	0.1252	0.3016	- -	SAbc
CGCG 11-103	11h27m57.5s	–01d12m40.1s	0.042687	1.5888	1.9545	- -	SA0
IC 992	14h18m14.9s	+00d53m28.0s	0.025965	0.3778	1.1523	43.75	SABc
UGC 5195	09h43m12.0s	+00d24m51.0s	0.025190	0.8237	0.9703	43.74	Sbc
UGC 5205	09h44m07.2s	–00d39m29.7s	0.005003	–1.6866	- - -	- -	SBm
UGC 5242	09h47m05.5s	+00d57m51.9s	0.006137	–0.1979	0.0223	- -	SBm
IC 1011	14h28m04.5s	+01d00m22.8s	0.025647	0.3966	0.6289	43.68	–
UGC 6608	11h38m33.2s	–01d11m04.2s	0.020776	0.8511	1.4847	43.52	SABab
MCG 0-30-7	11h32m45.4s	–00d44m27.7s	0.022379	0.4967	0.2987	- -	SBm
CGCG 12-54	11h40m06.4s	–00d50m15.7s	0.019591	–0.1357	- - -	- -	E
CGCG 12-27	11h34m39.1s	+00d07m29.1s	0.028791	0.2434	- - -	- -	SA0/a
CGCG 12-5	11h32m09.2s	–00d56m33.4s	0.026154	–0.0494	- - -	- -	SAB0
CGCG 12-53	11h40m06.2s	–00d54m05.0s	0.028712	0.6698	1.5266	- -	SAb
IC 716	11h39m03.3s	–00d12m21.6s	0.018078	0.6377	- - -	- -	Sbc
NGC 3720	11h32m21.8s	+00d48m17.0s	0.020068	0.1563	0.9369	44.09	SAa
NGC 5750	14h46m11.1s	–00d13m22.6s	0.005827	0.3941	- - -	42.52	SB0/a
NGC 5733	14h42m45.9s	–00d21m03.8s	0.005698	0.4660	0.0989	- -	dIn
UGC 9470	14h41m48.6s	+00d41m13.1s	0.006427	1.3992	- - -	- -	SBdm
UGC 9977	15h41m59.5s	+00d42m46.0s	0.006483	1.3629	0.1903	42.41	Sc
MCG 0-39-4	15h07m59.2s	+01d13m54.2s	0.035114	0.5962	1.5006	44.05	S?
UGC 9732	15h08m09.7s	+01d14m57.6s	0.035335	0.4407	0.7379	- -	SBb
CGCG 17-54	13h39m13.2s	–01d07m15.4s	0.014852	0.2651	0.3066	- -	Sb
CGCG 17-43	13h38m06.4s	+00d01m13.7s	0.022360	–0.1490	0.2262	- -	HII?
NGC 5887	15h14m43.9s	+01d09m15.4s	0.029286	0.1289	- - -	- -	SA0
UGC 10264	16h12m56.8s	–00d05m46.5s	0.030845	0.6339	- - -	43.88	SABcd
MCG 0-41-5	16h10m14.6s	+01d03m20.5s	0.027844	0.6427	- - -	- -	SABdm
IC 4229	13h22m26.1s	–02d25m05.7s	0.023181	0.2678	0.9835	43.83	SBb
UGC 10005	15h45m14.3s	+00d46m19.9s	0.012830	0.3854	- - -	- -	SAd
A1301-03	13h04m31.1s	–03d34m20.6s	0.004623	–0.2095	0.1498	- -	SABdm
UGC 10306	16h16m43.5s	+00d14m47.2s	0.030720	0.0906	- - -	- -	SABb
MK502	16h53m42.9s	+64d05m06.8s	0.041539	0.1778	- - -	- -	Compact
IC 1235	16h52m03.6s	+63d06m56.8s	0.010433	0.1460	0.0481	- -	–
IC 1248	17h11m40.1s	+59d59m44.2s	0.016699	0.3598	0.7844	- -	SBc

[a] Luminosity in unit of erg s^{-1}.

Table 5. Flux densities of emissions.

Name	*F4861*	*F5007*	*F6548*	*F6584*	*F6563*	*F6717*	*F6731*
NGC 3042	87.60	206.83	215.99	715.24	356.47	173.07	174.66
UGC 5238	221.14	343.76	50.40	131.92	839.97	136.81	100.51
UGC 7963	40.52	16.64	25.60	68.87	169.61	35.46	25.17
A1252+00	117.13	69.67	61.47	133.81	406.33	106.49	75.72
NGC 4668	77.33	111.44	25.37	62.83	247.01	50.40	40.74
CGCG 15-20	32.83	63.76	41.08	100.76	85.81	33.22	37.83
MCG 0-29-27	454.87	3623.94	474.27	1397.25	1894.18	476.63	436.90
UGC 6435	32.27	54.61	54.48	143.85	100.85	45.46	63.48
UGC 6340	59.64	113.27	52.29	133.68	159.19	93.57	83.84
UGC 6432	67.03	40.45	27.58	69.79	212.42	29.59	23.91
CGCG 11-100	84.60	59.61	48.37	170.48	382.18	53.53	41.48
MCG 0-29-29	205.59	60.20	100.57	340.95	950.97	155.27	115.74
UGC 9299	100.17	142.39	19.46	49.81	268.74	60.93	41.82
IC 1010	28.23	50.21	37.40	114.03	77.11	40.71	45.17
MCG 0-29-36	118.48	100.65	71.61	169.99	447.58	43.43	33.22
UGC 6402	262.24	321.97	90.41	255.23	1212.12	240.04	170.32
UGC 6457	74.76	119.94	6.10	19.30	209.89	47.78	35.90
MCG 0-30-4	24.88	10.97	7.94	23.57	53.15	7.72	7.94
MCG 0-29-28	85.01	26.07	32.01	90.03	245.07	40.70	28.08
NGC 3719	99.62	73.50	69.68	206.05	318.08	79.54	64.01
CGCG 11-103	176.13	597.52	371.61	1052.18	1027.92	186.33	192.54
IC 992	413.55	149.43	239.34	733.45	1800.94	195.61	155.79
UGC 5195	75.89	50.32	56.59	174.65	309.25	65.11	45.78
UGC 5205	0.88	4.33	3.68	11.91	8.45	1.88	3.18
UGC 5242	73.65	142.13	11.32	21.61	212.37	33.74	24.61
IC 1011	264.94	116.42	133.05	427.08	953.21	174.78	131.63
UGC 6608	144.86	51.48	115.72	339.64	712.22	116.92	101.07
MCG 0-30-7	41.99	31.64	12.77	30.72	133.92	42.33	27.34
CGCG 12-54	13.71	58.07	24.72	43.51	43.81	4.70	19.61
CGCG 12-27	14.47	11.71	8.74	15.70	20.60	7.53	3.79
CGCG 12-5	65.53	184.96	126.14	266.62	220.74	91.16	82.65
CGCG 12-53	198.49	40.59	113.06	327.10	990.92	123.50	93.72
IC 716	47.00	57.84	32.01	169.37	159.05	64.46	63.97
NGC 3720	180.55	38.49	78.30	233.36	726.85	66.07	53.76
NGC 5750	216.90	331.13	306.15	869.79	802.45	525.02	399.84
NGC 5733	223.31	505.47	27.75	83.83	662.12	132.27	88.91
UGC 9470	17.79	24.47	12.69	12.06	52.33	14.95	12.16
UGC 9977	51.81	29.84	16.95	49.62	158.83	48.37	33.27
MCG 0-39-4	855.21	292.04	764.47	2451.81	4229.11	752.21	658.27
UGC 9732	81.72	90.88	98.14	250.93	305.94	108.88	77.93
CGCG 17-54	78.90	28.70	24.87	86.00	252.37	57.94	38.02
CGCG 17-43	153.46	136.86	38.97	125.39	476.67	110.59	79.35
NGC 5887	64.82	110.90	122.43	299.64	182.45	124.74	108.50
UGC 10264	30.11	87.02	22.06	77.12	94.72	32.00	21.27
MCG 0-41-5	20.38	31.95	14.14	34.65	32.84	13.35	14.66
IC 4229	1039.08	189.08	562.62	1755.09	4254.76	538.92	442.83
UGC 10005	27.08	11.16	9.99	22.88	52.19	15.34	12.29
A1301-03	296.09	671.88	30.27	93.71	894.39	130.47	91.69
UGC 10306	51.46	92.14	89.49	254.92	173.67	103.60	83.59
MK502	23.63	13.44	11.75	32.05	51.36	10.20	7.92
IC 1235	233.19	210.91	60.58	170.31	678.74	180.12	126.67
IC 1248	176.12	43.94	68.81	216.49	670.64	115.54	76.33

Flux densities are in units of $10^{-17} \times$ erg s^{-1}cm^{-2}.

Table 6. Equivalent widths of emissions.

Name	*EW4861*	*EW5007*	*EW6548*	*EW6584*	*EW6563*	*EW6717*	*EW6731*
NGC 3042	0.31	0.67	0.71	2.33	1.17	0.52	0.53
UGC 5238	34.32	43.76	7.29	18.64	120.30	21.19	15.58
UGC 7963	3.52	1.30	2.14	5.69	14.12	2.54	1.80
A1252+00	3.73	1.91	1.87	3.99	12.25	4.05	2.89
NGC 4668	3.18	3.90	0.94	2.32	9.14	2.24	1.81
CGCG 15-20	0.50	0.92	0.64	1.56	1.33	0.47	0.54
MCG 0-29-27	6.72	45.88	6.41	18.07	25.12	7.14	6.55
UGC 6435	0.17	0.26	0.28	0.75	0.52	0.22	0.31
UGC 6340	0.39	0.70	0.33	0.86	1.02	0.58	0.52
UGC 6432	2.54	1.34	0.96	2.37	7.32	1.08	0.87
CGCG 11-100	1.92	1.29	1.04	3.66	8.22	1.20	0.93
MCG 0-29-29	6.48	1.77	3.02	10.27	28.62	6.24	4.66
UGC 9299	8.85	9.53	1.41	3.57	19.39	5.66	3.89
IC 1010	0.54	0.93	0.69	2.11	1.42	0.69	0.77
MCG 0-29-36	3.17	2.50	1.82	4.27	11.31	1.20	0.92
UGC 6402	10.34	10.50	3.10	8.52	41.06	9.12	6.47
UGC 6457	6.87	11.27	0.59	1.87	20.27	6.77	5.09
MCG 0-30-4	3.84	1.51	1.10	3.23	7.32	1.11	1.14
MCG 0-29-28	4.34	1.16	1.51	4.14	11.41	2.00	1.38
NGC 3719	2.36	1.65	1.61	4.74	7.33	1.89	1.52
CGCG 11-103	6.78	18.08	10.40	29.90	28.96	4.02	4.15
IC 992	12.18	4.12	6.86	20.75	51.35	6.75	5.38
UGC 5195	3.03	1.73	2.04	6.38	11.19	2.08	1.46
UGC 5205	0.12	0.43	0.41	1.40	0.97	0.36	0.62
UGC 5242	15.28	27.75	2.50	4.46	45.58	9.73	7.11
IC 1011	5.85	2.30	2.71	8.80	19.53	4.01	3.02
UGC 6608	4.85	1.58	3.56	10.33	21.78	3.25	2.81
MCG 0-30-7	7.33	5.35	2.14	4.95	22.07	8.23	5.32
CGCG 12-54	0.16	0.68	0.30	0.53	0.53	0.05	0.23
CGCG 12-27	1.37	1.00	0.76	1.36	1.80	0.65	0.33
CGCG 12-5	0.72	1.87	1.39	2.89	2.41	0.95	0.87
CGCG 12-53	8.12	1.36	3.89	11.10	33.90	4.49	3.41
IC 716	0.76	0.86	0.47	2.58	2.38	0.82	0.81
NGC 3720	6.26	1.18	2.49	7.38	23.08	2.70	2.20
NGC 5750	1.21	1.68	1.62	4.59	4.24	2.59	1.98
NGC 5733	7.76	16.69	0.95	2.85	22.59	6.07	4.09
UGC 9470	3.04	4.15	2.07	1.91	8.42	2.89	2.35
UGC 9977	4.18	2.33	1.25	3.75	11.81	3.26	2.24
MCG 0-39-4	11.36	3.61	9.36	30.28	51.96	9.85	8.62
UGC 9732	1.41	1.38	1.60	4.11	5.00	1.60	1.14
CGCG 17-54	5.97	1.78	1.69	5.95	17.28	5.03	3.30
CGCG 17-43	10.58	7.40	2.15	6.93	26.32	8.33	5.99
NGC 5887	0.48	0.71	0.84	2.04	1.25	0.77	0.67
UGC 10264	0.75	2.07	0.51	1.80	2.21	0.67	0.45
MCG 0-41-5	0.69	1.01	0.46	1.13	1.07	0.36	0.40
IC 4229	7.02	1.22	3.65	11.39	27.59	4.24	3.49
UGC 10005	2.90	0.98	0.93	2.08	4.80	1.62	1.30
A1301-03	43.31	77.93	3.82	11.99	113.47	27.64	19.48
UGC 10306	0.53	0.87	0.90	2.54	1.74	0.95	0.77
MK502	1.15	0.58	0.52	1.42	2.28	0.47	0.36
IC 1235	5.92	4.50	1.34	3.76	14.99	5.41	3.81
IC 1248	5.88	1.31	2.15	6.78	20.99	4.20	2.78

All equivalent wavelengths are in units of Å.

Table 7. Equivalent widths of absorptions.

Name	*EW3933*	*EW4200*	*EW4340*	*EW5173*	*EW4101*	*EW4300*	*EW4861*	*EW6563*	$D_n(4000)$
NGC 3042	17.63	11.38	10.38	9.19	0.70	2.96	3.84	1.64	1.83
UGC 5238	5.66	2.59	4.41	3.81	3.06	3.49	3.94	2.23	1.15
UGC 7963	8.56	4.73	6.29	5.95	2.92	3.84	4.13	2.11	1.29
A1252+00	7.50	3.24	5.42	4.71	4.07	4.43	4.78	2.35	1.20
NGC 4668	7.93	3.26	5.36	4.58	3.40	3.98	4.59	2.41	1.22
CGCG 15-20	17.81	10.89	10.41	9.36	0.59	2.96	3.72	1.49	1.87
MCG 0-29-27	9.33	4.63	6.46	5.86	2.47	3.57	3.95	2.10	1.29
UGC 6435	18.47	11.45	10.59	9.27	0.39	2.77	3.57	1.49	1.91
UGC 6340	18.07	10.64	10.18	8.41	0.55	2.90	3.42	1.51	1.86
UGC 6432	9.82	5.16	6.77	6.58	2.65	3.75	4.36	2.12	1.31
CGCG 11-100	9.62	4.82	6.63	6.14	2.81	3.82	4.29	2.09	1.33
MCG 0-29-29	2.82	1.84	3.38	3.31	4.81	4.05	4.71	1.75	1.12
UGC 9299	4.14	2.23	3.99	3.69	5.54	5.03	5.40	2.63	1.14
IC 1010	17.61	9.42	10.16	8.52	1.02	3.08	3.62	1.79	1.79
MCG 0-29-36	11.26	5.45	7.02	6.37	2.54	3.70	4.44	2.23	1.37
UGC 6402	2.90	2.05	3.31	3.43	5.84	5.15	5.67	2.64	1.13
UGC 6457	2.11	1.81	2.22	2.62	3.61	3.35	4.87	2.27	1.02
MCG 0-30-4	6.21	3.39	5.31	4.75	6.15	5.71	5.68	2.68	1.29
MCG 0-29-28	9.49	4.27	6.35	5.48	3.32	4.09	4.40	2.30	1.31
NGC 3719	13.46	6.50	8.46	7.39	1.52	3.12	3.61	1.89	1.48
CGCG 11-103	13.39	6.54	7.12	5.10	3.74	4.32	4.79	0.90	1.57
IC 992	5.67	3.18	4.50	4.55	3.51	3.84	4.73	2.29	1.14
UGC 5195	12.53	5.44	7.52	5.99	3.00	4.17	4.29	2.29	1.48
UGC 5205	8.57	4.92	6.47	7.45	2.61	3.40	5.07	1.70	1.21
UGC 5242	5.82	2.21	4.53	3.77	5.14	4.89	5.54	2.78	1.16
IC 1011	7.54	4.16	5.39	5.36	3.22	3.87	4.71	2.27	1.22
UGC 6608	10.75	5.37	7.11	6.21	2.24	3.50	3.82	2.11	1.37
MCG 0-30-7	6.50	3.34	4.58	4.07	4.62	4.66	5.30	2.66	1.20
CGCG 12-54	17.88	11.54	10.65	9.74	0.62	2.73	3.86	1.61	1.84
CGCG 12-27	14.44	6.79	8.44	7.12	2.02	3.67	3.98	2.13	1.55
CGCG 12-5	18.00	10.54	10.54	9.41	0.57	2.82	3.62	1.55	1.84
CGCG 12-53	7.22	4.08	5.21	4.89	3.39	4.00	4.53	2.32	1.21
IC 716	17.04	9.28	9.89	8.15	1.24	3.33	3.69	1.88	1.77
NGC 3720	4.97	3.47	4.25	5.10	2.86	3.38	4.66	2.09	1.09
NGC 5750	14.87	8.14	8.75	7.64	1.94	3.78	4.21	2.05	1.60
NGC 5733	3.82	2.29	3.31	3.32	3.85	3.84	4.86	2.42	1.08
UGC 9470	0.70	0.98	1.24	1.74	3.78	3.00	4.08	1.59	1.03
UGC 9977	4.89	3.35	4.95	4.35	7.40	6.43	6.19	2.78	1.29
MCG 0-39-4	7.53	4.29	5.67	5.64	2.98	3.79	4.30	2.09	1.23
UGC 9732	14.45	8.17	8.85	7.79	1.73	3.56	4.04	1.87	1.59
CGCG 17-54	5.70	2.74	4.32	4.16	2.77	3.31	4.18	2.24	1.11
CGCG 17-43	7.81	2.90	5.51	4.46	4.54	4.65	4.99	2.55	1.24
NGC 5887	18.58	11.54	10.71	9.12	0.47	2.85	3.52	1.55	1.92
UGC 10264	12.99	7.25	8.25	7.33	1.77	3.43	3.93	1.97	1.49
MCG 0-41-5	15.59	8.53	9.55	8.05	1.27	3.26	3.64	1.84	1.66
IC 4229	5.97	3.71	4.83	5.30	3.06	3.59	4.54	2.07	1.15
UGC 10005	8.13	3.49	5.53	4.69	3.39	3.98	4.44	2.38	1.24
A1301-03	3.64	2.40	3.30	3.62	3.84	3.91	5.22	2.25	1.04
UGC 10306	16.54	10.89	10.14	9.25	0.57	2.80	3.67	1.55	1.74
MK502	13.18	5.91	8.07	6.93	1.79	3.29	3.71	2.04	1.46
IC 1235	4.98	2.71	4.31	3.98	5.36	5.00	5.69	2.64	1.15
IC 1248	6.79	3.73	5.02	5.01	2.85	3.48	4.39	2.22	1.17

All equivalent wavelengths are in units of Å.